Experimental validation for time-domain fluorescence diffuse optical tomography of linear scheme

Feng Gao (高 峰), Limin Zhang (张丽敏), Jiao Li (李 娇), and Huijuan Zhao (赵会娟)

College of Precision Instrument and Optoeletronics Engineering, Tianjin University, Tianjin 300072

Received September 18, 2008

We present a full three-dimensional, featured-data algorithm for time-domain fluorescence diffuse optical tomography that inverts the Laplace-transformed time-domain coupled diffusion equations and employs a pair of appropriate transform-factors to effectively separate the fluorescent yield and lifetime parameters. By use of a time-correlation single-photon counting system and the normalized Born formulation, we experimentally validate that the proposed scheme can achieve simultaneous reconstruction of the fluorescent yield and lifetime distributions with a reasonable accuracy.

OCIS codes: 170.3880, 170.3660, 170.6280, 170.6960, 170.3010, 170.6920.
doi: 10.3788/COL20080612.0889.

As near infrared light can travel several centimeters in tissue, fluorescence diffuse optical tomography (FDOT) with the aid of specific fluorescent probes promises to open new pathways for the characterization of biological processes in living animals at cellular and molecular levels[1,2]. Several approaches have been proposed for recovering the fluorescent yield and/or lifetime distributions based on finite light measurements collected at the tissue boundary[2−9]. In FDOT, the yield imaging can provide the location information of biological fluorophores, while the lifetime one offers further chemical messages about the surroundings, such as pH, enzyme, and oxygen, etc. In principle, lifetime detection can be performed in either the time-domain (TD) technique or the frequency-domain (FD) one. Because typical fluorescence lifetime is very short, FD measurement generally requires a modulation frequency of up to 1 GHz and higher for molecular imaging of small animals to obtain an enough signal-to-noise ratio (SNR). This is not technically achievable yet as well as impractical due to exponential decay of the alternating current (AC) amplitude with the frequency[10,11]. In contrast, the TD technique offers the potential advantages of directly measuring lifetime and has the favorite performances of simultaneously recovering of fluorescent yield and lifetime distributions, as well as resolving multiple components[12]. Thus, it is necessary that FDOT modality be extended to time domain. In TD mode, the reconstruction approaches can be performed using either the full time-resolved scheme or the featured-data one. Although the former has been shown in simulative investigations to generate images with much higher quality than the latter, it is currently impractical to the realistic three-dimensional (3D) cases due to a high computation cost. As a result, various featured-data algorithms are preferable[2,12−14].

We describe here a full 3D, featured-data scheme for TD FDOT which has been verified to be reasonably noise-robust and computationally efficient[12], and present its validation using a time-resolved transmission experiment on a solid phantom. In our approach, a pair of appropriate Laplace-transformed factors is employed to extract the featured information on the temporal profiles obtained with the scanning mode of a single-channel time-correlation single-photon counting (TCSPC) system. The data-type in a formulation of the ratio of the Laplace-transformed emission signals to the excitation ones (the normalized Born ratio) is used for its independence of the source intensity and less sensitivity to the systematic errors. In addition, this normalized Born ratio eliminates the requirement for accurate calibration of the temporal-origin in TD measurement and also exhibits a high robustness to the uncertainties of highly optically heterogeneous background.

In TD-FDOT, light propagation and fluorescence generation in tissues can be described using the coupled TD diffusion equations. Its Laplace-transformed expression is given as[2,12,13]

$$\begin{aligned}&\left[-\nabla\cdot\kappa_{\mathrm{x}}(\mathbf{r})\nabla+(\mu_{\mathrm{ax}}(\mathbf{r})c+\beta)\right]\Phi_{\mathrm{x}}(\mathbf{r},\mathbf{r}_{\mathrm{s}},\beta)\\&=\delta(\mathbf{r}-\mathbf{r}_{\mathrm{s}}),\\&\left[-\nabla\cdot\kappa_{\mathrm{m}}(\mathbf{r})\nabla+(\mu_{\mathrm{am}}(\mathbf{r})c+\beta)\right]\Phi_{\mathrm{m}}(\mathbf{r},\mathbf{r}_{\mathrm{s}},\beta)\\&=c\Phi_{\mathrm{x}}(\mathbf{r},\mathbf{r}_{\mathrm{s}},\beta)\eta\mu_{\mathrm{af}}(\mathbf{r})/\left[1+\beta\tau(\mathbf{r})\right],\end{aligned}\tag{1}$$

where subscripts "x" and "m" denote the excitation and emission wavelengths, respectively; β is the transform factor; c is the speed of light in the medium; $\Phi_\nu(\mathbf{r},\mathbf{r}_{\mathrm{s}},\beta)$ $(\nu=\mathrm{x},\mathrm{m})$ is the Laplace transform of the TD photon density $\Phi_\nu(\mathbf{r},\mathbf{r}_{\mathrm{s}},t)$. For working with a TCSPC system, $\Phi_\nu(\mathbf{r},\mathbf{r}_{\mathrm{s}},\beta)\approx\sum_{n=0}^{N_{\mathrm{t}}}-(\Phi_v^{n+1}(\mathbf{r},\mathbf{r}_{\mathrm{s}},t_{n+1})-\Phi_v^n(\mathbf{r},\mathbf{r}_{\mathrm{s}},t_n))\Delta t/\beta$, where N_{t} is the number of time channels, Δt is the time-bin of TCSPC (i.e., sampling time interval), and $\Phi_v^n(\mathbf{r},\mathbf{r}_{\mathrm{s}},t_n)$ is the photon count in the nth time-bin. The optical properties involved are the absorption coefficient $\mu_{\mathrm{a}\nu}(\mathbf{r})$, the reduced scattering coefficient $\mu'_{\mathrm{s}\nu}(\mathbf{r})$, and the diffusion coefficient $\kappa_\nu(\mathbf{r},t)=c/[3\mu'_{\mathrm{s}\nu}(\mathbf{r})]$. The fluorescence properties are the fluorescent lifetime $\tau(\mathbf{r})$ and the fluorescent yield $\eta\mu_{\mathrm{af}}(\mathbf{r})$ that is the product of the fluorophore's quantum efficiency (which depends on the type of fluorophore and

the chemical environment) and its absorption coefficient (which depends on the fluorophore's concentration).

With the normalized Born-ratio formulation, where the emission flux is normalized by the excitation one, an integral equation is obtained according to Eq. (1)[13,15,16]:

$$\frac{I_{\mathrm{m}}(\mathbf{r}_{\mathrm{d}},\mathbf{r}_{\mathrm{s}},\beta)}{I_{\mathrm{x}}(\mathbf{r}_{\mathrm{d}},\mathbf{r}_{\mathrm{s}},\beta)}=\frac{\Theta}{I_{\mathrm{x}}(\mathbf{r}_{\mathrm{d}},\mathbf{r}_{\mathrm{s}},\beta)}\times\int_{\Omega}cG_{\mathrm{m}}(\mathbf{r}_{\mathrm{d}},\mathbf{r},\beta)\,\Phi_{\mathrm{x}}(\mathbf{r},\mathbf{r}_{\mathrm{s}},\beta)\,x(\mathbf{r},\beta)\,\mathrm{d}\Omega,\qquad(2)$$

where $I_{\nu}(\mathbf{r}_{\mathrm{d}},\mathbf{r}_{\mathrm{s}},\beta)$ represents the measurable flux at the boundary site $\mathbf{r}_{\mathrm{d}}$ with the excitation source at $\mathbf{r}_{\mathrm{s}}$, Θ is a factor associated with the normalized light-source strength and the total attenuation of the filters, $x(\mathbf{r},\beta)=\eta\mu_{\mathrm{af}}(\mathbf{r})/[1+\beta\tau(\mathbf{r})]$ and $G_{\mathrm{m}}(\mathbf{r}_{\mathrm{d}},\mathbf{r},\beta)$ is the Green function of emission diffusion equation. For reconstruction, the integral equation is volumetrically discretized into a number of voxels, which yields a set of linear equations. Among many different approaches to tackling the linear inversion which is typically underdetermined and ill-posed problem, the algebraic reconstruction technique (ART) is employed here due to its modest memory requirement for large inverse problems and the attained high computation speed. The reconstructed unknown quantity $x(\mathbf{r},\beta)$ is a function of the fluorescence yield and lifetime as well as the transform-factor β. We empirically select a pair of factors $\beta_{1,2}=\mp1/[1/(\mu_{\mathrm{ax}}^{(\mathrm{B})}c)+1/(\mu_{\mathrm{am}}^{(\mathrm{B})}c)+\tau^{(\mathrm{B})}]$ (where the superscript "B" denotes the background) and the corresponding reconstructed $x(\mathbf{r},\beta_1)$ and $x(\mathbf{r},\beta_2)$. Thus the fluorescent yield and lifetime parameters can be effectively separated as

$$\eta\mu_{\mathrm{af}}(\mathbf{r})=\frac{(\beta_1-\beta_2)\,x(\mathbf{r},\beta_1)\,x(\mathbf{r},\beta_2)}{\beta_1x(\mathbf{r},\beta_1)-\beta_2x(\mathbf{r},\beta_2)},$$

$$\tau(\mathbf{r})=-\frac{x(\mathbf{r},\beta_1)-x(\mathbf{r},\beta_2)}{\beta_1x(\mathbf{r},\beta_1)-\beta_2x(\mathbf{r},\beta_2)}.\qquad(3)$$

To validate the proposed method, we prepare the transmission mode TD-FDOT experiments on a solid rectangular phantom, as shown in Fig. 1. The excitation light source is a pulsed diode laser (BLHP-700, Becker and Hickl Gmbl, Germany) at 660 nm with a repetition rate of 50 MHz. The laser light is collimated and coupled into a source fiber with a core diameter of 62.5 μm and numerical aperture (NA) of 0.22 to scan the phantom on one wall. The emitted light is collected by a detection fiber with a core diameter of 500 μm and NA of 0.37 on the opposite wall and sent to a cooled photomultiplier tube (PMT) which is coupled to a TCSPC module (SPC-134, Becker and Hickl Gmbl, Germany) for time-resolved detection of both the excitation and emission photons. For the fluorescence detection, the signals pass through three long-pass filters (light transmissivity is 50% at 700 ± 5 nm, and more than 90% at 715 nm) before entering the PMT. For the TCSPC setup in our experiment, the time-to-amplitude converter (TAC) range is set to 70 ns and the analog-to-digital converter (ADC) resolves the TAC signal into 4096 time-bins. This leads to a sampling time interval of 17.1 ps. To properly work with the TCSPC system, the strength of the light source is greatly reduced in the excitation measurement as compared to the emission one, while the signal acquisition (integration) time is fixed at 10 s. This difference in the laser power is calibrated in the image reconstruction process. The whole setup is placed in a dark box to shield the stray light. The data analysis and image reconstruction are performed with custom-developed software in Matlab.

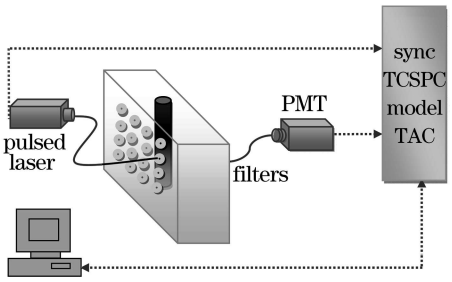

Fig. 1. Experimental setup.

The rectangular solid with a dimension of $10\times7\times2.5$ (cm) phantom is made from polyformaldehyde. Its optical properties are determined to be $\mu_{\mathrm{a}}=0.0038$ mm^{-1} and $\mu_{\mathrm{s}}'(\mathbf{r})=0.938$ mm^{-1} by a curve-fitting between the measured and model-predicted time-resolved data. The initial background fluorescence properties are empirically set to $\eta\mu_{\mathrm{af}}(\mathbf{r})=0.00001$ mm^{-1} and $\tau(\mathbf{r})=10000$ ps. To simulate fluorescent targets embedded in the tissue, a cylindrical hole of 0.5 cm in diameter and 6 cm in height is drilled in the midway of the thickness and filled with a mixed medium that consists of 1% intralipid solution and Cy5.5 agent (the peak excitation and emission at 670 and 710 nm, respectively). The 16 source sites on one wall of the slab are arranged in a 4×4 grid with a tip-to-tip

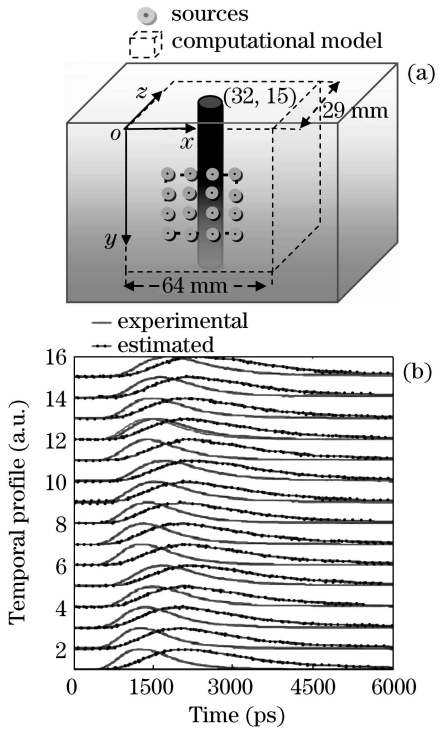

Fig. 2. (a) Sketch of phantom and computational model; (b) normalized temporal profiles along detection channels for the first source.

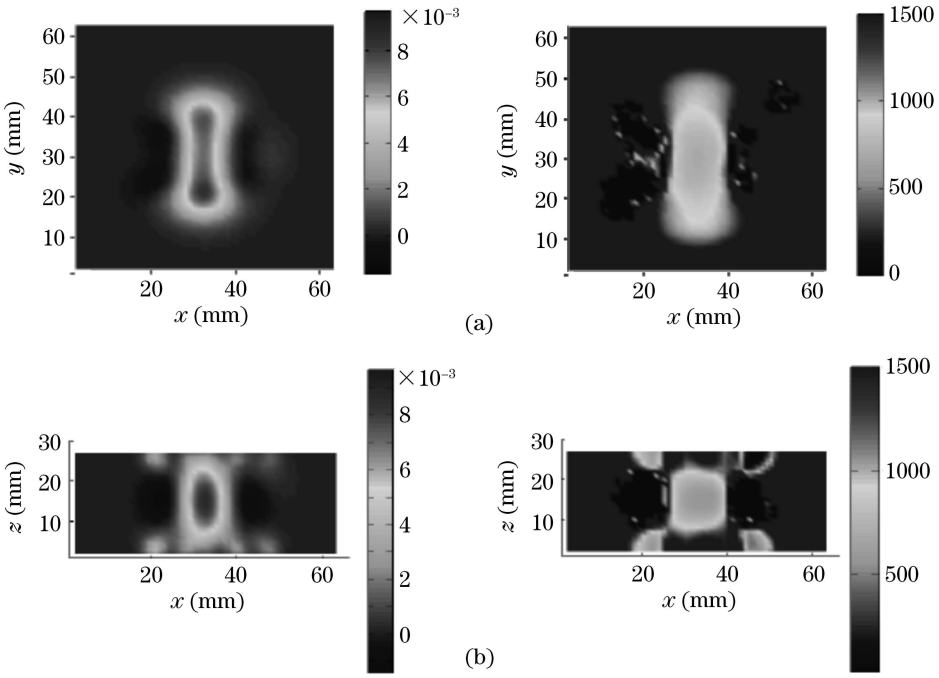

Fig. 3. Reconstructed images of fluorescent yield (left) and lifetime (right) from the experimental data. (a) Vertical slice at $z = 15$ mm; (b) horizontal slice at $y = 30$ mm.

distance of 7 mm along both the x- and y-directions, and the 16 detection sites are arranged in the same grid pattern on the opposite wall with co-axial correspondence along the z-direction. This placement results in a total of 16×16 time-resolved measurements at the excitation and emission wavelengths over a field of view (FOV) of 21×21 (mm), which are used to construct the raw dataset for the subsequent tomography reconstruction. As shown in Fig. 2(a), to reduce the computational cost, we choose a dimension of $64 \times 64 \times 29$ (mm) around the FOV in the forward model, i.e., a finite-element method solution to the photon diffusion equation with an extrapolated boundary condition[11]. The cylindrical target is therefore centered at $x = 32$ mm and $z = 15$ mm in the given coordinate system. Figure 2(b) illustrates the normalized temporal profiles measured at the 16 detection sites as the first source irradiates the phantom. The same discretization mesh of cubic element as that for the forward calculation is used for the image reconstruction, with a voxel size of $1.5 \times 1.5 \times 1.5$ (mm). The number of ART iteration in the linear inversion is fixed to 20 with the relaxation parameter being 0.1. This empirical setting shows a good balance between the convergence speed and image quality.

Figure 3(a) shows a vertical slice (x-y plane) at $z = 15$ mm of the reconstructed fluorescence yield and lifetime distributions, and Fig. 3(b) presents the horizontal slice (x-z plane) at $y = 30$ mm of the reconstructed distribution. As can be seen, the reconstructed results show that this technique is able to recover the target location and shape accurately, and in terms of the quality of yield and lifetime images, the yield is more satisfying. However, the reconstructed diameter of the target is slightly overestimated, especially for the lifetime images. We believe that this issue is caused by the ill-posedness of the inverse problem, which can be greatly improved by denser source and detection sampling. The reconstructed optical properties around the target exhibit some differences from the background, which might be briefly interpreted as the result of breakdown in the first-order diffusion theory at the interface between drastically distinct optical media. In addition, some edge artifacts around the source and detection boundaries can be observed in Fig. 3(b). In this study, we measured the photons at the excitation wavelength without fluorescence filters and again confirmed that the influence of the emission photons is negligible[16]. Other factors that might adversely affect the imaging performance include the deviation of experimentally measured optical properties from the actuality, the instability of the laser power between the excitation and emission measurements and the temporal delay and distortion of the signals incurred by the filters, etc. An investigation in depth is required for the solutions to these issues and for the quantitation assessment of the reconstruction.

In summary, we have experimentally validated a linear, featured-data scheme for TD-FDOT. The results show that the proposed method is noise-robust and computationally efficient and can simultaneously reconstruct fluorescence yield and lifetime images with reasonable quality. This work provides a promising FDOT method and is important for small animal imaging.

This work was supported by the National Natural Science Foundation of China (No. 60578008, 60678049), the National Basic Research Program of China (No. 2006CB705700), and Tianjin Municipal Government of China (No. 07JCYBJC06600). F. Gao's e-mail address is gaofeng@tju.edu.cn.

References

1. V. Ntziachristos, C.-H. Tung, C. Bremer, and R. Weissleder, Nat. Med. **8,** 757 (2002).
2. F. Gao, W. Liu, and H. Zhao, Chin. Opt. Lett. **4,** 595 (2006).
3. F. Yang, Y. Ma, F. Gao, and H. Zhao, Acta Opt. Sin. (in Chinese) **28,** 1571 (2008).
4. L. Zhang, H. He, F. Gao, and H. Zhao, Acta Opt. Sin. (in Chinese) **28,** 1262 (2008).
5. M. A. O'Leary, D. A. Boas, X. D. Li, B. Chance, and A. G. Yodh, Opt. Lett. **21,** 158 (1996).
6. A. B. Milstein, S. Oh, K. J. Webb, C. A. Bouman, Q. Zhang, D. A. Boas, and R. P. Millane, Appl. Opt. **42,** 3081 (2003).
7. V. Y. Soloviev, J. McGinty, K. B. Tahir, M. A. Neil, A. Sardini, J. V. Hajnal, S. R. Arridge, and P. M. French, Opt. Lett. **32,** 2034 (2007).
8. S.-H. Han and D. J. Hall, Opt. Lett. **33,** 1035 (2008).
9. S. C. Davis, H. Dehghani, J. Wang, S. Jiang, B. W. Pogue, and K. D. Paulsen, Opt. Express **15,** 4066 (2007).
10. V. Y. Soloviev, K. B. Tahir, J. McGinty, D. S. Elson, M. A. A. Neil, P. M. W. French, and S. R. Arridge, Appl. Opt. **46,** 7384 (2007).
11. F. Gao, H. Zhao, L. Zhang, Y. Tanikawa, A. Marjono, and Y. Yamada, Opt. Express **16,** 13104 (2008).
12. F. Gao, H. Zhao, Y. Tanikawa, and Y. Yamada, Opt. Express **14,** 7109 (2006).
13. L. Zhang, F. Gao, H. He, and H. J. Zhao, Opt. Express **16,** 7214 (2008).
14. S. Lam, F. Lesage, and X. Intes, Opt. Express **13,** 2263 (2005)
15. A. Soubret, J. Ripoll, and V. Ntziachristos, IEEE Trans. Med. Imaging **24,** 1377 (2005).
16. V. Ntziachristos and R. Weissleder, Opt. Lett. **26,** 893 (2001).